Neurobiology of Pain 16 (2024) 100164

Contents lists available at ScienceDirect

Neurobiology of Pain

journal homepage: www.sciencedirect.com/journal/neurobiology-of-pain

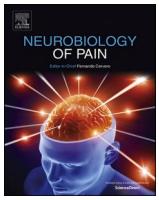

Original Research

Quantitative orbital tightening for pain assessment using machine learning with DeepLabCut

Saurav Gupta, Akihiro Yamada, Jennifer Ling, Jianguo G. Gu *

Department of Anesthesiology and Perioperative Medicine, School of Medicine, University of Alabama at Birmingham, Birmingham, AL 35294, United States

ARTICLE INFO

Keywords:
Pain
Grimace scale
Orbital tightening
Artificial intelligence
Machine learning
DeepLabCut

ABSTRACT

Pain assessment in animal models is essential for understanding mechanisms underlying pathological pain and developing effective pain medicine. The grimace scale (GS), facial expression features in pain such as orbital tightening (OT), is a valuable measure for assessing pain in animal models. However, the classical grimace scale for pain assessment is labor-intensive, subject to subjectivity and inconsistency, and is not a quantitative measure. In the present study, we utilized machine learning with DeepLabCut to annotate the superior and inferior eyelid margins and the medial and lateral canthus of the eyes in animals' video images. Based on the annotation, we quantified the eyelid distance and palpebral fissure width of the animals' eyes so that the degree of OT in animals with pain could be measured and described quantitatively. We established criteria for the inclusion and exclusion of the annotated images for quantifying OT, and validated our quantitative grimace scale (qGS) in the mice with pain caused by capsaicin injections in the orofacial or hindpaw regions, the Nav1.8-ChR2 mice following orofacial noxious stimulation with laser light, and the oxaliplatin-treated mice following tactile stimulation with a von Frey filament. We showed that both the eyelid distance and the palpebral fissure width were shortened significantly in the animals in pain compared to the control animals without nociceptive stimulation. Collectively, the present study has established a quantitative orbital tightening for pain assessment in mice using DeepLabCut, providing a new tool for pain assessment in preclinical studies with mice.

Introduction

Pain assessment in rodent models is important for understanding the mechanisms of pathological pain and developing effective pain medication for human patients suffering from chronic intractable pain (Deuis et al., 2017). However, pain assessment in animals is difficult due to the lack of verbal communication between animals and humans. Nevertheless, similar to humans who show facial expressions such as orbital tightening when in pain (Prkachin, 1992; Craig et al., 2001), most mammals, like humans, exhibit facial expressions of pain (Onuma et al., xxxx). Accordingly, researchers have developed a grimace scale (GS) to analyze facial expressions of pain in animals such as mice, rats, horses, cats, pigs, and other mammals (Onuma et al., xxxx; Langford et al., 2010; Sotocinal et al., 2011; Dalla Costa et al., 2014; Holden et al., 2014; Di Giminiani et al., 2016; Hager et al., 2017). The rodent GS is a tool developed to assess pain in mice and rats based on facial expressions with 5 features: orbital tightening, nose bulge, cheek bulge, ear position change, and whisker position change (Langford et al., 2010; Sotocinal et al., 2011; Tuttle et al., 2018). However, research has found that inter-rater reliability of GS, measured by the intraclass correlation coefficient (ICC), is high for orbital tightening but less so for the other 4 features (Zhang et al., 2019; Arnold et al., 2023; Oliver et al., 2014; Philips et al., 2017). Thus, orbital tightening is considered to be the most prominent and reliable indicator among the 5 features of GS for pain assessment (Zhang et al., 2019; Arnold et al., 2023; Oliver et al., 2014; Philips et al., 2017).

The rodent GS has been used for assessing spontaneous and ongoing pain in rodent models of inflammation pain, chemotherapy-induced pain, and neuropathic pain, significantly advancing preclinical pain research (Onuma et al., xxxx; Langford et al., 2010; Sotocinal et al., 2011; Philips et al., 2017; Akintola et al., 2017). Traditionally, researchers performed GS for pain assessment by manually analyzing all five features from a large number of images (Langford et al., 2010; Sotocinal et al., 2011). This manual GS is time-consuming and labor-intensive and suffers from subjectivity and inconsistency. Recently, researchers have explored the application of machine learning techniques to automate the prediction of the GS in mice (Tuttle et al., 2018; Arnold et al., 2023; Andresen et al., 2020). Automated GS has demonstrated

* Corresponding author.
E-mail address: jianguogu@uabmc.edu (J.G. Gu).

https://doi.org/10.1016/j.ynpai.2024.100164
Received 23 July 2024; Received in revised form 16 August 2024; Accepted 26 August 2024
Available online 2 September 2024
2452-073X/© 2024 The Author(s). Published by Elsevier Inc. This is an open access article under the CC BY-NC-ND license (http://creativecommons.org/licenses/by-nc-nd/4.0/).

good accuracy in assessing animal pain (Tuttle et al., 2018; Arnold et al., 2023; Andresen et al., 2020) and has overcome subjectivity and inconsistency encountered in the manual GS. However, the automated GS methods used in previous studies were technically sophisticated and difficult to adopt for broad use by many pain research labs. More recently, a study reported the development of PainFace software to simplify, standardize, and scale up mouse grimace analyses, a cloud-based software platform using machine learning (McCoy et al., 2024). However, all previous manual and automated GS use arbitrarily defined scores, e.g., obvious (score of 2), moderate (score of 1), and no eye tightening (score of 0), for the five features of grimace scale (Langford et al., 2010; Sotocinal et al., 2011; Tuttle et al., 2018; McCoy et al., 2024). The scores of the GS in these previous studies were thus not quantitative measurements even though the average scores could be calculated and numerical values were then presented (Langford et al., 2010; Sotocinal et al., 2011; Tuttle et al., 2018; McCoy et al., 2024).

Orbital tightening, GS's most prominent and reliable feature in pain assessment (Zhang et al., 2019; Arnold et al., 2023; Oliver et al., 2014; Philips et al., 2017), may be quantified and used for assessing pain in animals. A higher degree of orbital tightening usually occurs with more severe pain in humans (Prkachin, 1992; Craig et al., 2001), and this intensity coding of pain with the degree of orbital tightening may also be present in animals in pain. Quantification of orbital tightening can be made by measuring the eyelid distance, the distance between the inferior eyelid margin and the superior eyelid margin. Additionally, palpebral fissure width, the distance between the medial and lateral canthus, may also become shortened in animals with pain (Prkachin, 1992; Craig et al., 2001). However, this quantification has never been performed previously, most likely because it is extremely time-consuming to perform quantification manually. DeepLabCut, an open-source toolbox that builds on a state-of-the-art animal pose estimation algorithm (Mathis et al., 2018; Nath et al., 2019), may be used for automated quantification of orbital tightening and pain assessment. DeepLabCut is a markerless pose estimation method that utilizes transfer learning with deep neural networks to track user-defined features in animals performing various behaviors (Mathis et al., 2018; Nath et al., 2019). DeepLabCut has been used to investigate sensory, motor, and social behaviors in different animals (Dooley et al., 2020; Piotrowski et al., 2024; Mykins et al., 2024; Bidgood et al., 2024; Reddy et al., 2023). In the context of automated quantification of orbital tightening for pain assessment in animals, the eyelid distances and palpebral fissure width need to be measured. Through machine learning with DeepLabCut, the superior and inferior margins of eyelids and the medial and lateral canthus in the images of animals may be recognized and precisely labeled automatically. This may offer a reliable and time-efficient approach to quantify orbital tightening for pain assessment.

In the present study, using machine learning with DeepLabCut, we quantified eyelid distances and palpebral fissure widths in mice without nociceptive stimulation, mice in pain induced by subcutaneous injection of capsaicin, pain caused by blue laser light stimulation in the Nav1.8-ChR2 mice (Yamada et al., 2023), and pain in oxaliplatin-treated mice following mechanical stimulation. We quantitatively demonstrated orbital tightening in animals following the nociceptive stimulations.

Materials and methods

Animals: Heterozygous Nav1.8-ChR2 mice were created by crossing Scn10aCre and Ai32(RCL-ChR2(H134R)/EYFP) transgenic mice. Scn10aCre mice, provided by Dr. John Wood from University College London and transferred from Dr. Stephen Waxman's lab at Yale University, were crossed with Ai32 mice obtained from Jackson Labs. Adult male mice aged between 13 to 21 weeks were used in this study. All animal care and experimental procedures adhered to the guidelines established by the National Institutes of Health (NIH) for the care and use of experimental animals. Approval for the experimental protocols was obtained from the Institutional Animal Care and Use Committee (IACUC) at the University of Alabama at Birmingham.

The setup of sheltering tubes for orbital tightening assessment: We have recently implemented the sheltering tube method to facilitate reliable assessment of orofacial nociceptive responses using the von Frey test, acetone spray test, and optogenetic test (Gupta et al., 2024). In the present study, we used this method to accommodate testing animals to investigate orbital tightening (OT) in mice. In brief, each sheltering tube consists of a one-end closed cylinder plastic tube with an inner diameter of 3.8 cm and a depth of 11 cm. The actual depth of the sheltering tube was adjusted to 4.6–5.6 cm by adding the lids of Falcon tubes to accommodate mice of different body sizes for OT behavioral assessment. Each sheltering tube was mounted on a stand placed on a lab bench, with the sheltering tube slightly tiled so that the opening of the sheltering tube angled 15° upward. The height from the lab bench to the sheltering tubs was 20 to 50 cm. Mice underwent two sessions, and each was acclimated for ~ 30 min in the home cages on the bench of the behavioral testing room and 45 min of habituation in sheltering tubes for two consecutive days. On the OT behavioral assessment day, mice were brought to the behavioral test room and acclimated for 30 min in the home cages. Mice were then placed in the sheltering tubes. After a quick accommodation with animals' head stably positioned in the opening of sheltering tubes, video images were recorded at 1920x1080 resolution and a rate of 24 frames per second using a Logitech Brio webcam. Unless otherwise indicated, each experiment recorded the video images for 10 min (14400 images). The video camera was positioned at the same level as the animal's head and 12 cm away from the opening of the sheltering tube, and it was tilted at an angle of 15 degrees toward the right side of the animal. After completing the habituation mentioned above or the orofacial behavioral tests described below, the sheltering tubes were thoroughly cleaned with lab detergent or 70 % ethanol and then water for the next uses.

Drug administration: To induce orofacial pain in mice, capsaicin (5——10 μl, 10 mM in saline) was subcutaneously injected into the orofacial region. A control group of mice received an equivalent volume of saline injection. In a separate group of mice, capsaicin was subcutaneously injected into the hindpaw regions in the same doses. Video images were taken 10 min after the injection of capsaicin. In a different set of experiments, mice received daily intraperitoneal injections of oxaliplatin (2 mg/kg) for five consecutive days (total dose 10 mg/kg) to create a chemotherapy-induced pain model. Video images were taken 7 days after the last dose of oxaliplatin.

Blue light stimulation to whisker pad regions of mice in sheltering tubes: To investigate OT in response to blue light stimulation, the Nav1.8-ChR2 mice were placed in the sheltering tube. Video images were taken 1 min before and 1 min after a blue laser beam was applied to the whisker pad region with an optical fiber (diameter: 0.2 mm: Laserglow technologies). The light intensities were calibrated with an optical power and energy meter (PM100D, Thorlab) driven by a stimulator (Master-8, A.M.P.I., Jerusalem, Israel). For our experiments, laser light stimulation was applied one time to the whisker pad regions at the intensities of 60 mW/mm^2, and the duration of each stimulus was 50 ms.

The von Frey test in orofacial regions for mice in sheltering tubes: Mice injected with oxaliplatin or saline (control) were used in this set of experiments.

To examine the mechanical sensitivity in the orofacial regions of testing animals, von Frey filaments were applied on the right side of the orofacial region. The von Frey filament of 0.07 g (North Coast Medical, NC12775-99) was applied to the orofacial regions when the head of the mouse stayed still in the sheltering tube, and OT was determined following the tactile stimulation. The video images were taken prior to and immediately after the von Frey filament stimulation, and the video images after the stimulation was taken for 1 min.

Deep machine learning and labeling of eyelids: Video images (1920×1080 pixels, 24 fps) of the facial regions of mice in sheltering tubes were recorded for 10 min for each animal. DeepLabCut 2.3.0 (https://github.com/DeepLabCut/DeepLabCut), a Python-based

software, was used for video image analysis (Mathis et al., 2018; Nath et al., 2019). Video image frames were first extracted from 2 to 5 mice, 20 frames from each animal, and their right eye's superior and inferior eyelid margins and the medial and lateral canthus were manually labeled as "body parts" for DeepLabCut to learn. A training dataset was generated from these labeled images. A deep learning neural network was trained over 100,000 iterations to establish a model for tracking the annotated body parts. The trained model was then applied to all the video images of experimental animals. The data containing the body parts' positions in the CSV format were output to Excel for further processing to calculate the eyelid distance and the palpebral fissure width of the right eye.

Data processing and calculation of the eyelid distance and palpebral fissure width: The CSV files were opened with Excel, and each data point included video image frame number, name of body parts (e.g., superior eyelid margins), coordinate of each body part, and detection likelihood or accuracy. Based on the coordinates of the body parts, we calculated the pixel distances between the superior and inferior eyelid margins (eyelid distance) and the distance between the medial and lateral canthus of the eyes (palpebral fissure width) using Excel. In a new Excel spreadsheet, we included columns for video image frame number, eyelid distance, palpebral fissure width, and detection likelihood for the 4 positions (superior and inferior eyelid margins and medial and lateral canthus) of the right eyes. Data points with a detection likelihood below 0.95 at any of the 4 positions were excluded. Data points from labeling left eyes (wrong labeling) were also excluded. Finally, the pixel distances were converted into the actual distance in millimeters.

Statistical Analysis: Following the calculation of the eyelid distance and the palpebral fissure width using DeepLabCut and Excel, as described above, the final data points were imported into GraphPad Prism 10.1.2 software for statistical analysis. Histograms for the eyelid distance and palpebral fissure width were plotted using the GraphPad Prism with a bin width set at 0.1 mm. Mean eyelid distances and palpebral fissure width were calculated, and statistical comparisons were performed based on the mean distances. Results are presented as Mean ± SEM. Statistical significance was determined using one-way ANOVA or Student's *t*-test, with ns denoting no significant difference, *p < 0.05, **p < 0.01, and ***p < 0.001 representing significance levels.

Results

To establish a reliable experimental condition for assessing one of the important grimace scale parameters, orbital tightening, we employed the sheltering tube method (Gupta et al., 2024), focusing on the orofacial regions of Nav1.8-ChR2 mice for behavioral tests (Fig. 1). The reason for using Nav1.8-ChR2 mice was because, in some experiments, we used blue laser light to induce orofacial pain and determine orbital tightening in these animals. The sheltering tubes simulate a hole-like environment, aligning with mice's and other rodents' innate behavior to reside in holes. When placed in sheltering tubes, mice could freely turn their bodies, positioning their heads outward after a few adjustments (Gupta et al., 2024). This orientation allowed for optimal visualization and video recording of the eyelids, facilitating the measurement of orbital tightening as outlined in Fig. 1. After two acclimation sessions, the mice adapted quickly to the sheltering tubes and did not exhibit observable stress behaviors, creating a stable condition for investigating orbital tightening behavioral responses (Fig. 1). Using the sheltering tube method, we recorded 10-minute videos of the mice at 24 frames per second. Utilizing the DeepLabCut, we labeled the superior and inferior eyelid margins and the medial and lateral canthus (Fig. 1). Several types of labeled images were found in our experiments using DeepLabCut, and each type has different likelihood values (1 being 100 % accuracy), as represented in Fig. 2A-E. Most labeled images showed precise labeling on the superior and inferior eyelid margins and

Figure 1

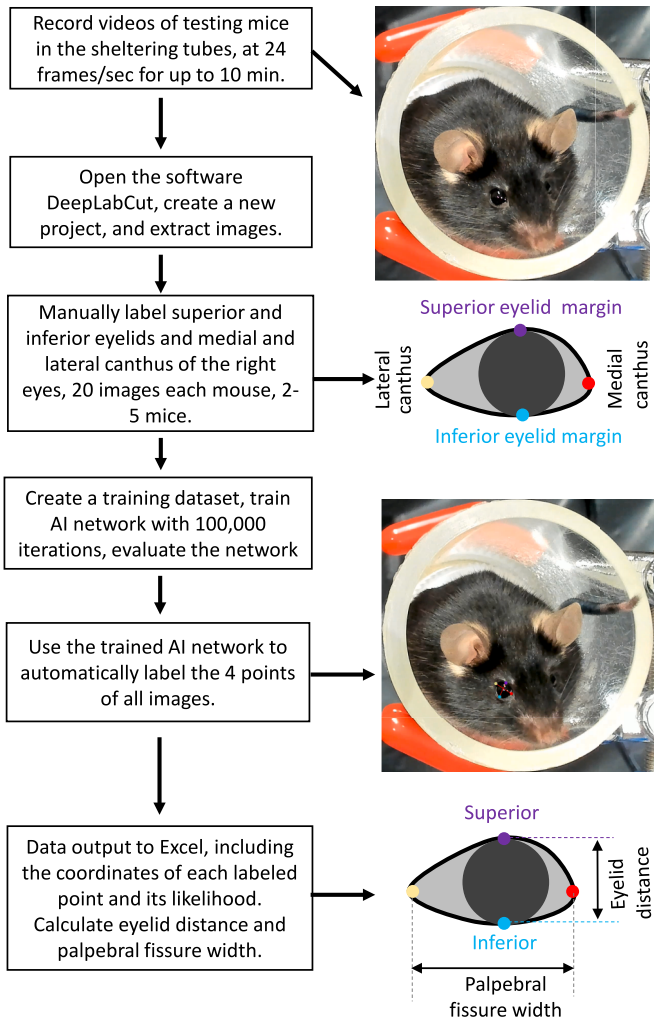

Fig. 1. Steps for evaluating orbital tightening in mice using machine learning with DeepLabCut. The flowchart illustrates using machine learning with DeepLabCut to measure eyelid distance and palpebral fissure width in mice to evaluate orbital tightening. First, mice were placed in the sheltering tubes. The orofacial regions of the testing mice were then video recorded at 24 frames/sec for up to 10 min. The video images were extracted by the DeepLabCut to create a new project. The superior and inferior eyelid margins, as well as the medial and lateral canthus of the right eyes of the mice images, were manually labeled, 20 frames of images per mouse with a total of 2 to 5 mice. A training dataset was generated, and an artificial intelligence (AI) network of the DeepLabCut was trained with the labeled images for 100,000 iterations. The trained artificial intelligence network was then used to automatically label the superior and inferior eyelid margins and the medial and lateral canthus of the right eyes of all video images collected in the experiments. Data were then imported to Excel, which included the coordinates of each labeled point and their likelihood (accuracy). The distance between the superior and inferior eyelid margins was the eyelid distance, and the distance between the medial and lateral canthus of the right eye was the palpebral fissure width. The present study used eyelid distance and palpebral fissure width as measures of eye tightening.

the medial and lateral canthus of the right eyes, with likelihood values of ≥ 0.95 (Fig. 2A). This type of labeled image accounted for 87 % of total images (Fig. 2F). Some images showed no or incomplete labeling due to incorrect head positions (Fig. 2B) or fuzzy images caused by a rapid head movement (Fig. 2C), and labeling for these images showed very low likelihood values. This type of labeled image accounted for 12 % of total images (Fig. 2F). In a few images, the left eyes were partially

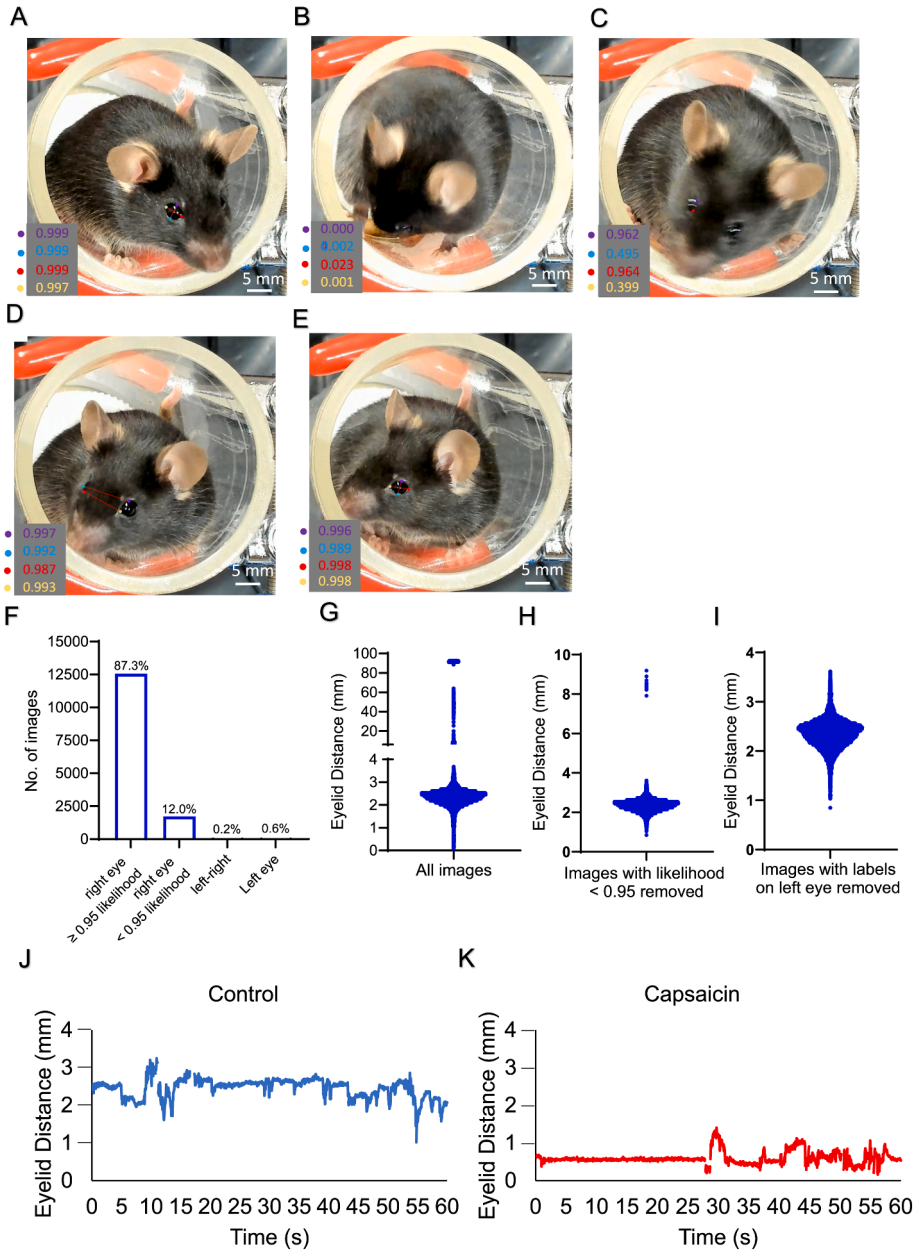

Fig. 2. Inclusion and exclusion criteria for the images labeled by the DeepLabCut. A-E) Example images of a normal mouse with its head in 5 different positions resulted in different labeling by the DeepLabCut. The first image showed the superior (purple circle) and inferior (blue circle) eyelid margins, as well as the medial (red circle) and lateral (orange circle) canthus of the right eye of the animal that was accurately labeled. The likelihood value was > 0.99 at each labeled point (**A**). The likelihood values were shown in the left corner of the image. The 2nd and 3rd images showed missing or incomplete labeling due to an incorrect head position (**B**) or the rapid head movement that caused a fuzzy image (**C**), and the likelihood values were low at the putatively labeled points. The 4th and 5th images showed the cross labeling of both right and left eyes (**D**) or the left eye only (**E**) of the animal due to the head position with the left eye shown in the images, but the right eye was only partially shown (**D**) or missing (**E**) in the images. The labeling likelihood value was > 0.98 for each point. **F**) Graph shows the number and percentage of images that were right eyes with labeling likelihood ≥ 0.95 (1st bar), right eyes with labeling likelihood < 0.95 (2nd bar), and cross labeling of both right and left eyes (3rd bar) or labeling of left eyes (4th bar). **G)** Plot of the eyelid distances calculated from all 14,400 images recorded in 10 min without excluding the incorrectly labeled images. **H)** Plot of eyelid distances after excluding the images with labeling likelihood values < 0.95. **I)** Plot of eyelid distances from 12,568 images (87.3 %) after excluding the images with labeling likelihood values < 0.95 and those with left eyes labeled. **J&K)** Eyelid distances over 60 s in a mouse without (control, **J**) and a different mouse following capsaicin injection (capsaicin, **K**). Capsaicin was injected subcutaneously into the cheek of the animal. (For interpretation of the references to colour in this figure legend, the reader is referred to the web version of this article.)

(Fig. 2D) or completely labeled (Fig. 2E), and high likelihood values could be shown for these labeled images (Fig. 2D&E). These labeled images accounted for 0.8 % of total images (Fig. 2F). Fig. 2G showed the calculated eyelid distance from all the images video-recorded for 10 min in a testing animal, showing a broad distribution with some data points that were unrealistic as eyelid distances (Fig. 2G). After the labeled images with likelihood values smaller than 0.95 (Fig. 2B&C) had been removed, most unrealistic data points disappeared (Fig. 2H). Subsequent removal of the images whose left eyes were partially and completely labeled (Fig. 2D&E) led to the calculated eyelid distances clustered in the range from 2 to 3 mm (Fig. 2I). Therefore, through the aforementioned image analysis, we established data inclusion and exclusion criteria for measuring eyelid distance and palpebral fissure width using the DeepLabCut, and these criteria were used for all the

experiments described below.

Fig. 2J&K shows examples of eyelid distance over a minute of video images recorded in a control animal (without capsaicin injection) and an animal after a subcutaneous capsaicin injection in the orofacial region. In the control animal (Fig. 2J), the eyelid distance was from 2 to 3 mm most of the time, and sometimes the eyelid distance was reduced below 2 mm, representing a brief eye close. In contrast, in the capsaicin-injected animal, eyelid distance was under 1 mm most of the time, indicating sustained eye tightening (Fig. 2K).

We quantified the eyelid distances under normal conditions (baseline), following saline injection or subcutaneous capsaicin injection into the orofacial region in mice. Fig. 3A&B shows two control animals, one in normal condition (Fig. 3A) and another following saline injection (Fig. 3B), and no orbital tightening was observed in these control animals. Fig. 3C shows an animal injected with capsaicin, and orbital tightening was observed. We quantified the eyelid distances (Fig. 3D&E). Fig. 3D is an example of the histogram of the frequency distribution of the measured eyelid distances in three mice, one under baseline condition, another after saline injection, and a third after the capsaicin injection. The frequency distribution showed a narrow range in the eyelid distance with a peak at approximately 2.5 mm for both mice in the baseline condition and after saline injection (Fig. 3D). In contrast, a large leftward shift in the frequency distribution was observed in the mouse's eyelid distance after capsaicin injection, with a peak at approximately 0.6 mm (Fig. 3D). The average eyelid distance was 2.35 ± 0.07 mm (n = 8) observed in saline-injected mice, which was not significantly different from the eyelid distance of 2.29 ± 0.18 mm (n = 8 mice) measured at baseline (Fig. 3E). However, following capsaicin injection, the eyelid distance significantly decreased to 0.94 ± 0.41 mm (n = 8, Fig. 3E), indicating pronounced orbital tightening after capsaicin injection to induce pain in orofacial regions. Additionally, to a smaller degree, a leftward shift in the frequency distribution was observed for the palpebral fissure width of the right eyes. The average palpebral fissure width was 3.23 ± 0.20 mm (n = 8) observed in saline-injected mice, which was not significantly different from the palpebral fissure width of 3.29 ± 0.09 mm (n = 8 mice) measured at baseline (Fig. 3G). However, following capsaicin injection, the average palpebral fissure width significantly decreased to 2.85 ± 0.45 mm (n = 8, Fig. 3G).

We investigated whether orbital tightening occurs when capsaicin is injected into the hindpaw region to produce pain in distal regions. Fig. 4A shows no orbital tightening in a mouse following a subcutaneous injection of saline in the hindpaw region. Fig. 4B shows a clear orbital tightening in a mouse after a subcutaneous capsaicin injection in the hindpaw region. Fig. 4C shows the frequency distribution of the eyelid distances for the mouse in Fig. 4A (saline control) and Fig. 4B (capsaicin-injected). There was a leftward shift in the distribution of eyelid distances in the capsaicin-injected mouse compared to the saline-injected mouse. The average eyelid distance following saline injection in the hindpaw region was 2.64 ± 0.05 mm (n = 5), which significantly decreased to 1.93 ± 0.13 mm (n = 5) after capsaicin injection (Fig. 4D), indicating orbital tightening in response to pain induced by capsaicin. A notable leftward shift was not observed in the distribution of the palpebral fissure width in the capsaicin-injected mouse compared to the saline-injected mouse (Fig. 4E). The average palpebral fissure width following saline injection in the hindpaw region was 3.36 ± 0.08 mm (n = 5), which slightly decreased to 3.20 ± 0.13 mm (n = 5) after capsaicin injection (Fig. 4F).

We investigated whether orbital tightening occurred in Nav1.8-ChR2 mice following noxious stimulation by a blue laser beam applied to the whisker pad region. Nav1.8-ChR2 mice express channelrhodopsin-2 (ChR2) in Nav1.8-expressing TG neurons, and these TG neurons are mostly nociceptors. We applied the blue laser light stimulation at 60 mW/mm^2 intensity to the whisker region, which immediately induced nocifensive avoidance responses. This was followed by a prolonged orbital tightening (Fig. 5A&B). As shown in Fig. 5A, there was no orbital tightening in the mice before the laser light stimulation (pre-stimulation). In contrast, orbital tightening could be observed within 1 min following blue laser beam stimulation (post-stimulation, Fig. 5B). Fig. 5C shows the frequency distribution of eyelid distances before and within 1 min following the laser light stimulation, displaying a leftward shift after the stimulation. The average eyelid distance before stimulation was 2.557 ± 0.27 mm (n = 7), significantly reduced to 1.89 ± 0.13

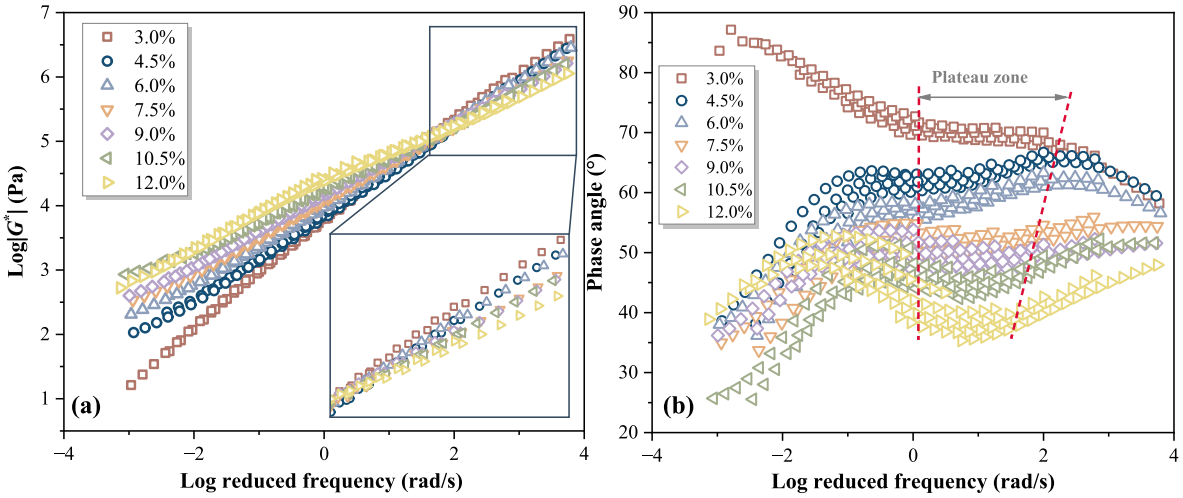

Fig. 3. Quantifying orbital tightening induced by capsaicin injection in the orofacial region. A-C) Images show the positions of the superior and inferior eyelid margins as well as the medial and lateral canthus of the right eye labeled by machine learning with DeepLabCut in a mouse without injection (baseline control, **A**), a mouse after saline injection in the cheek (saline control, **B**), and a mouse after capsaicin injection into the cheek (**C**). The line between the superior and inferior eyelid margins shows the eyelid distance. Eye tightening was seen in the mouse after capsaicin injection. **D**) Frequency distribution of eyelid distance for images in 10 min for a mouse of baseline condition (grey), a mouse after saline injection (blue), and a mouse after capsaicin injection (red). The bin width of the histogram is 0.1 mm. **E**) Average eyelid distances at baseline (n = 8, grey), after saline injection (n = 8, blue), and after capsaicin injection (n = 8, red). **F**) Frequency distribution of palpebral fissure images in 10 min for a mouse of baseline condition (grey), a mouse after saline injection (blue), and a mouse after capsaicin injection (red). The bin width of the histogram is 0.1 mm. **G**) Average palpebral fissure width at baseline (n = 8, grey), after saline injection (n = 8, blue), and after capsaicin injection (n = 8, red). Saline or capsaicin was injected subcutaneously. Data represent individual observations and mean ± SEM; *p < 0.05, ***p < 0.001; ns, no significant difference, one-way ANOVA with Sidak's post hoc test. (For interpretation of the references to colour in this figure legend, the reader is referred to the web version of this article.)

Figure 4

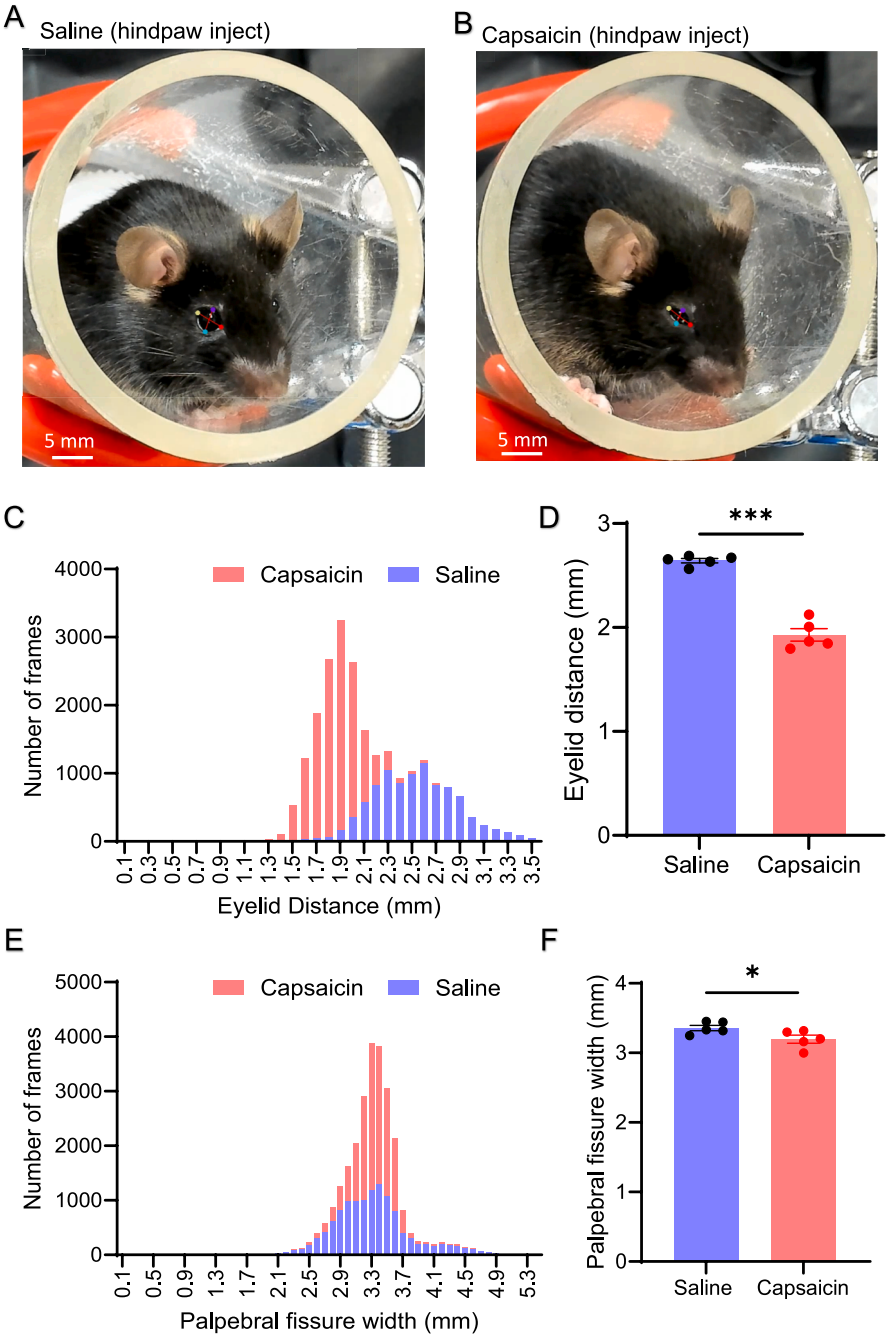

Fig. 4. Quantifying orbital tightening induced by capsaicin injection in the hindpaws. A&B) Images show the positions of the superior and inferior eyelid margins as well as the medial and lateral canthus of the right eye labeled by machine learning with DeepLabCut in a mouse after subcutaneous saline injection (saline, **A**) and a mouse after subcutaneous capsaicin injection in the hindpaws (capsaicin, **B**). Eye tightening was seen in the mouse after the capsaicin injection. **C**) Frequency distribution of eyelid distance for images in 10 min for a mouse after saline injection (blue) and a mouse after capsaicin injection (red). The bin width of the histogram is 0.1 mm. **D**) Average eyelid distances after saline (n = 5, blue) and capsaicin (n = 5, red) injections. **E**) Frequency distribution of palpebral fissure width for images in 10 min for a mouse after subcutaneous saline injection (blue) and a mouse after subcutaneous capsaicin injection (red). The bin width of the histogram is 0.1 mm. **F**) Average palpebral fissure width after saline (n = 5, blue) and capsaicin (n = 5, red) injections. Data represent individual observations and mean ± SEM, *p < 0.05, ***p < 0.001, Student's *t*-test. (For interpretation of the references to colour in this figure legend, the reader is referred to the web version of this article.)

mm (n = 7) after blue laser light stimulation (Fig. 5D). Fig. 5E shows the frequency distribution of the palpebral fissure width of the right eye before and after the laser light stimulation in an animal, displaying a leftward shift after the stimulation. The average palpebral fissure width before stimulation was 3.73 ± 0.31 mm (n = 7), significantly reduced to 3.32 ± 0.29 mm (n = 7) after blue laser light stimulation (Fig. 5F). This reduction in eyelid distances and palpebral fissure width indicates a significant orbital tightening in response to pain induced by the laser light stimulation that excited Nav1.8-expressing nociceptors.

Chemotherapy drugs such as oxaliplatin induce neuropathic pain, often resulting in mechanical allodynia triggered by gentle touch. We investigated whether orbital tightening could occur in mice following oxaliplatin treatment. However, we did not observe any significant difference in the eyelid distances between animals without and with

Figure 5

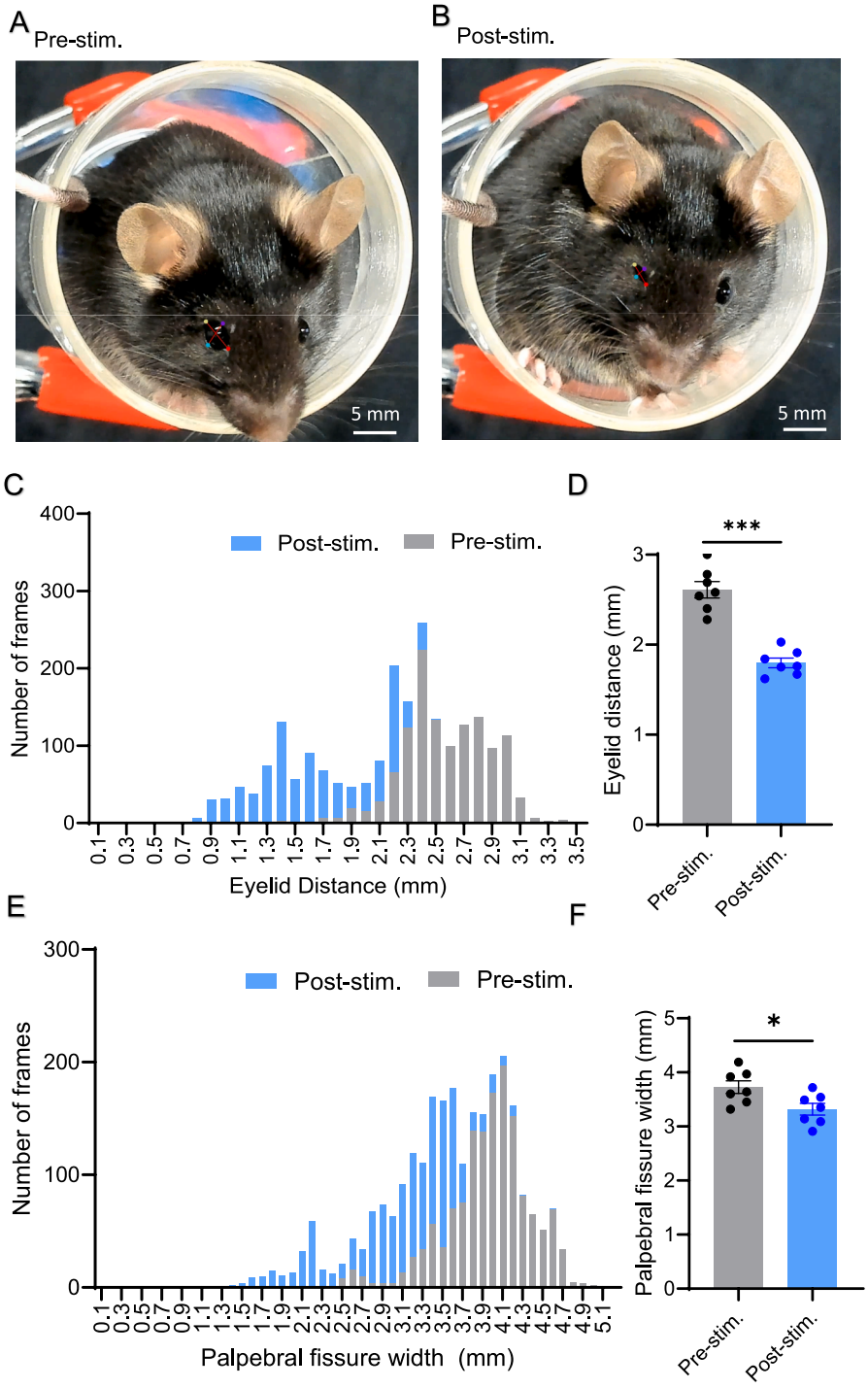

Fig. 5. Quantifying orbital tightening induced by blue laser light stimulation in the orofacial regions. A&B) Images show the positions of the superior and inferior eyelid margins as well as the medial and lateral canthus of the right eye labeled by machine learning with DeepLabCut in a mouse before (pre-stim., **A**) and following blue laser light stimulation (post-stim., **B**). Animals were Nav1.8-ChR2 mice, and blue laser light stimulation induced orbital tightening (**B**). **C**) Frequency distribution of eyelid distance for images in 1 min for a mouse before (pre-stim., grey) and after (post-stim., blue) blue laser light stimulation to the orofacial regions. The bin width of the histogram is 0.1 mm. **D**) Average eyelid distances before (n = 7, pre-stim.) and after blue laser light stimulation (n = 7, post-stim.). **E**) Frequency distribution of the palpebral fissure width for images in 1 min for a mouse before (pre-stim., grey) and after (post-stim., blue) blue laser light stimulation to the orofacial regions. The bin width of the histogram is 0.1 mm. **F**) Average palpebral fissure width before (n = 7, pre-stim.) and after blue laser light stimulation (n = 7, post-stim.). Blue laser light was applied to the orofacial regions at 60 mW/mm2. Data represent individual observations and mean ± SEM, *p < 0.05, ***p < 0.001, paired Student's *t*-test. (For interpretation of the references to colour in this figure legend, the reader is referred to the web version of this article.)

oxaliplatin injection (Fig. 6A-D). As shown in Fig. 6C, there was no shift in the frequency distribution of eyelid distances for oxaliplatin-treated mice compared to control mice without oxaliplatin treatment. The average eyelid distance in the mice without oxaliplatin was 2.56 ± 0.11 mm (n = 5), which was not significantly different from the 2.44 ± 0.25 mm (n = 5) observed after oxaliplatin treatment (Fig. 6D). In Fig. 6E, there was no shift in the palpebral fissure width frequency distribution for oxaliplatin-treated mice compared to the control mice without oxaliplatin treatment. The average palpebral fissure width in the mice without oxaliplatin was 3.44 ± 0.12 mm (n = 5), which was not significantly different from the 3.41 ± 0.12 mm (n = 5) observed after oxaliplatin treatment (Fig. 6F).

Next, we determined whether orbital tightening may be induced by mechanical stimulation applied to orofacial regions of oxaliplatin-treated animals. In this set of experiments, the von Frey filament of 0.07-g was applied 1 or 2 times to the orofacial regions of the testing mice. In the mice without oxaliplatin treatment, there was no orbital tightening following the mechanical stimulation with the von Frey filament (Control post-VF, Fig. 7A, D&E). Similarly, there was no orbital tightening in the oxaliplatin-treated mice before the mechanical stimulation (Oxa. pre-VF, Fig. 7B, D&E). However, the orbital tightening was evidenced in the oxaliplatin-treated mice within 1 min following mechanical stimulation with the 0.07-g von Frey filaments (Oxa. post-VF, Fig. 7C, D&E). As shown in Fig. 7D, the peak of the frequency distribution of eyelid distances was leftward shifted in oxaliplatin-treated mice (Oxa. post-VF) compared to the control without oxaliplatin treatment but with von Frey filament stimulation (control post-VF) or oxaliplatin-treated mice without von Frey filament stimulation (Oxa. pre-VF). The average eyelid distance was 2.52 ± 0.09 mm (n = 5) in mice without oxaliplatin treatment but with von Frey filament stimulation (control post-VF), and 2.56 ± 0.24 mm (n = 5) in oxaliplatin-treated mice without von Frey filament stimulation (Oxa. pre-VF), which significantly decreased to 1.175 ± 0.20 mm (n = 5) in oxaliplatin-treated mice following von Frey filament stimulation (Oxa. post-VF, Fig. 7E). In Fig. 7F, the peak of the frequency distribution of the palpebral fissure width was slightly leftward shifted in oxaliplatin-treated mice with von Frey filament stimulation (Oxa. post-VF) compared to control mice without oxaliplatin treatment but with von Frey filament stimulation (control post-VF) or oxaliplatin-treated mice without von Frey filament stimulation (Oxa. pre-VF). The average palpebral fissure width was 3.47 ± 0.16 mm (n = 5) in control mice (control post-VF) and 3.42 ± 0.18 mm (n = 5) in oxaliplatin-treated mice without von Frey filament stimulation (Oxa. pre-VF), which significantly decreased to 2.95 ± 0.31 mm (n = 5) in oxaliplatin-treated mice within 1 min following von Frey filament stimulation (Oxa. post-VF, Fig. 7G).

Discussions

In the present study, we used machine learning with the DeepLabCut to quantify orbital tightening, an important parameter of the grimace scales, to assess orofacial pain in Nav1.8-ChR2 mice. This study is aligned with the growing interest in utilizing artificial intelligence for video image analysis in behavioral research to achieve reliable outcomes without subjectivity (Tuttle et al., 2018; Arnold et al., 2023; Andresen et al., 2020; McCoy et al., 2024). For the first time, our study provides a quantitative and automated method to measure orbital tightening for pain assessment in mice. This new approach may help advance preclinical pain research in orofacial regions and other body parts, facilitating the development of effective pain medicine.

In the present study, we used the sheltering tube method implemented recently by our group to accommodate the testing mice (Gupta et al., 2024). The mice adapted to the sheltering tube rapidly without observable stress behaviors (Gupta et al., 2024), and they usually kept their heads towards the video camera. This facilitated optimal visualization and video recordings of the eyelids of the testing animals. With machine learning, the Deeplabcut software (Mathis et al., 2018; Nath et al., 2019) could precisely label eyelids in most recorded video images. In the present study, the right eyes were chosen for machine learning. After the training, our artificial intelligence network could selectively label the superior and inferior eyelid margins and the medial and lateral canthus of the right eyes. However, the accuracy of the labeling could be affected by the incorrect head position and head movement of the testing mice, which had lower likelihood values and accounted for approximately 10 % of the recorded images. Also, left eyes were occasionally labeled in a small fraction of images (<1%). We excluded those incorrectly labeled images in the present study using Excel's data sorting function. We used the labeled images with likelihood values equal to or greater than 0.95, which accounted for nearly 90 % of total images. By doing the aforementioned data analysis and selection, we ensured a high accuracy for quantifying eye tightening in animals with pain in the present study.

In the present study, we quantitatively investigated orbital tightening in animals following capsaicin injection in the right cheek and hind paws, blue laser light stimulation of the orofacial regions, and mechanical stimulation of the orofacial regions in animals treated with oxaliplatin. Capsaicin could directly excite nociceptors by activating TRPV1 channels to induce pain (Caterina et al., 1997), and it could also trigger the release of neuropeptides from nociceptors to induce neurogenic inflammation (Kilo et al., 1997). Consistent with the idea that orbital tightening is an important parameter of grimace scales of pain (Prkachin, 1992; Craig et al., 2001; Langford et al., 2010; Sotocinal et al., 2011), we showed the shift in the frequency distribution of the eyelid distance toward the left side (shorter eyelid distance) and the average eyelid distance was significantly reduced. Similarly, we observed the shift in the frequency distribution of the palpebral fissure width toward the left side (shorter width), and the average palpebral fissure width was significantly reduced. However, the degree of the reduction of palpebral fissure width was less compared with the reduction of the eyelid distance, suggesting that the eyelid distance is a more sensitive indicator of eye tightening. Since capsaicin injection in the cheek induced tissue swelling in the facial region, one may argue that eye tightening following capsaicin injection was due to tissue swelling rather than pain. However, we also observed the shift in the frequency distribution of the eyelid distance toward the left side (shorter eyelid distance) and the reduction of the average eyelid distance in mice following capsaicin injection in the hindpaws. Interestingly, the degree of eye tightening in mice with capsaicin injected in the hindpaws was less than in those injected with capsaicin in the cheek. These may be due to the differences in the severity of pain experienced by the animals with capsaicin injected in different body sites. Alternatively, tissue swelling in the orofacial region may partially contribute to eye tightening in experiments with capsaicin injected into the cheek. The capsaicin-induced orbital tightening in the present study is consistent with previous studies showing that ongoing inflammatory pain could result in orbital tightening (Langford et al., 2010; Sotocinal et al., 2011). However, in a previous study, the GS score was not found to be significantly affected in mice injected with capsaicin in the hindpaws (Sotocinal et al., 2011). The discrepancy between the present study and the previous study could be due to the differences in the data analysis of GS. Our quantitative measurement of orbital tightening with eyelid distance as an indicator should be more sensitive than previous binary grimace scales for assessing pain induced by capsaicin (Sotocinal et al., 2011). The discrepancy could also be due to using different lines of mice in the present and previous studies (Sotocinal et al., 2011).

In the present study, we used blue laser light to stimulate nociceptors since the Nav1.8-ChR2 mice used in our experiments expressed ChR2 in nociceptors, which could be excited by blue laser light (Yamada et al., 2023; Yamada et al., 2024). In our previous study, we applied the blue laser light at the intensity of 60 mW/mm^2, which elicited nocifensive avoidance at 100 % response frequency (Yamada et al., 2023; Gupta et al., 2024). After a brief blue laser light stimulation to the orofacial

Figure 6

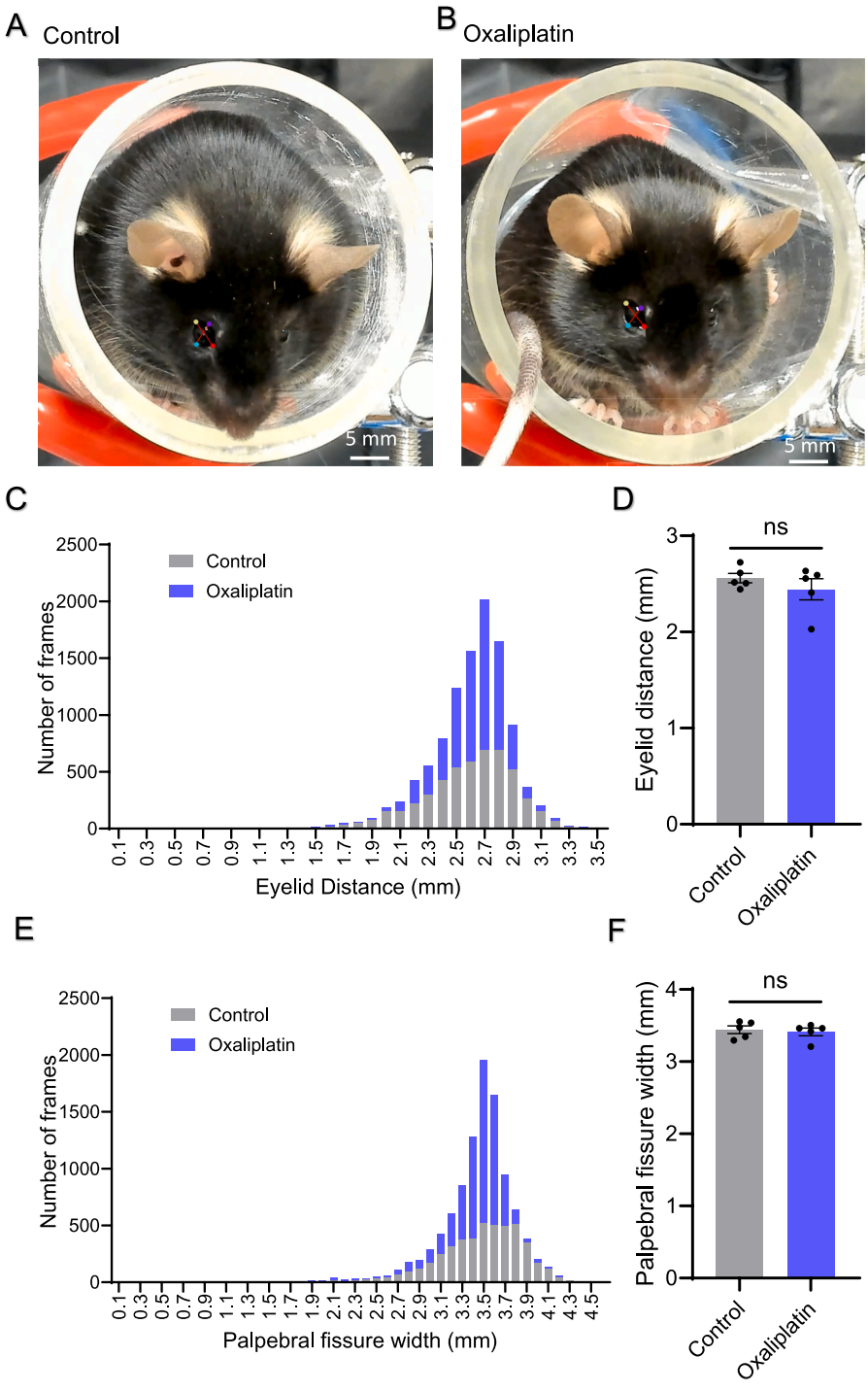

Fig. 6. Quantifying eyelid distance in mice following oxaliplatin treatment. A&B) Images show the positions of the superior and inferior eyelid margins as well as the medial and lateral canthus of the right eye labeled by machine learning with DeepLabCut in a mouse without (control, **A**) and with the treatment of oxaliplatin (**B**). **C**) Frequency distribution of eyelid distance for images in 5 min for a mouse without (control, grey) and with oxaliplatin treatment (blue). The bin width of the histogram is 0.1 mm. **D**) Average eyelid distances for mice without (control, n = 5, grey) and with oxaliplatin treatment (n = 5, blue). **E**) Frequency distribution of palpebral fissures width for images in 5 min for a mouse without (control, grey) and with oxaliplatin treatment (blue). The bin width of the histogram is 0.1 mm. **F**) Average palpebral fissure width for mice without (control, n = 5, grey) and with oxaliplatin treatment (n = 5, blue). Oxaliplatin was *i.p.* injected at the daily dose of 2 mg/kg for 5 consecutive days, and experiments were performed 7 days after the last dose of oxaliplatin treatment. Data represent individual observations and mean ± SEM, ns, not significantly different, Student's *t*-test. (For interpretation of the references to colour in this figure legend, the reader is referred to the web version of this article.)

Figure 7

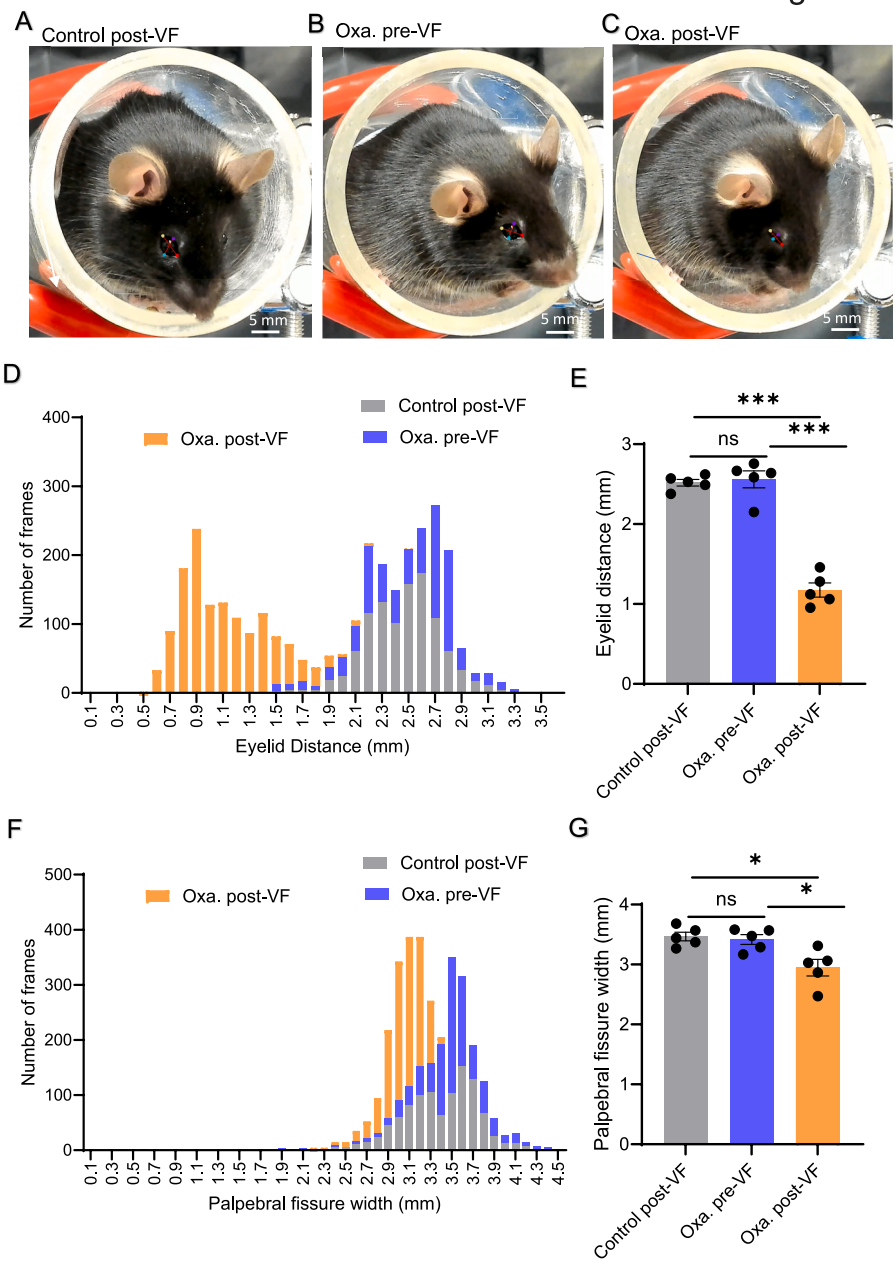

Fig. 7. Quantifying orbital tightening in oxaliplatin-treated mice following mechanical stimulation with von Frey filaments. A-C) Images show the positions of the superior and inferior eyelid margins as well as the medial and lateral canthus of the right eye labeled by machine learning with DeepLabCut in a mouse without oxaliplatin treatment but after mechanical stimulation with the 0.07-g von Frey filament (control post-VF, **A**), an oxaliplatin-treated mouse before mechanical stimulation with the von Frey filament (Oxa Pre-VF, **B**), and oxaliplatin-treated mouse after mechanical stimulation with the von Frey filament (Oxa post-VF, **C**). Eye tightening was seen in the oxaliplatin-treated mouse after the mechanical stimulation (Oxa. post-VF). **D**) Frequency distribution of the eyelid distance for images in 1 min for a mouse after mechanical stimulation with the von Frey filament (Control post-VF), an oxaliplatin-treated mouse before mechanical stimulation (Oxa pre-VF, blue), and an oxaliplatin-treated mouse after the mechanical stimulation with the von Frey filament (Oxa post-VF, orange). The bin width of the histogram is 0.1 mm. **E**) Average eyelid distances of the Control post-VF (n = 5, grey), Oxa pre-VF (n = 5. Blue), Oxa pre-VF (n = 5, blue) and Oxa post-VF (n = 5, orange). **F**) Frequency distribution of palpebral fissure width for images in 1 min for a mouse after mechanical stimulation with the von Frey filament (Control post-VF), an oxaliplatin-treated mouse before mechanical stimulation (Oxa pre-VF, blue), and an oxaliplatin-treated mouse after the mechanical stimulation with the von Frey filament (Oxa post-VF, orange). The bin width of the histogram is 0.1 mm. **G**) Average palpebral fissure width of the control post-VF (n = 5, grey), Oxa pre-VF (n = 5. Blue), Oxa pre-VF (n = 5, blue) and Oxa post-VF (n = 5, orange). Data represent individual observations and mean ± SEM; *p < 0.05, ***p < 0.001; ns, no significant difference, one-way ANOVA with Sidak's post hoc test. (For interpretation of the references to colour in this figure legend, the reader is referred to the web version of this article.)

regions, we observed a leftward shift of the frequency distribution and the reduction of average eyelid distance and palpebral fissure width, and the eye tightening lasted approximately 1 min. The detection of eye tightening after the end of laser light stimulation indicates that painful facial expression could remain for an extended time after the termination of nociceptive stimulation by the laser light. One possibility for this extended painful facial expression could be the release of neuropeptides from Nav1.8-ChR2-positive nociceptors to continue to excite nociceptors for an extended time.

Oxaliplatin is a chemotherapy drug known to induce neuropathic

pain, including mechanical and cold allodynia in humans (Argyriou et al., 2008) and experimental animals (Gupta et al., 2024; Abd-Elsayed et al., 2015). Interestingly, we did not observe significant orbital tightening in oxaliplatin-treated animals when tactile stimulation was not applied. The lack of measurable eye tightening in our study could be that spontaneous pain occurred infrequently as an ongoing paroxysm in the oxaliplatin-treated mice, so the quantification of orbital tightening did not capture significant changes in the eyelid distances and palpebral fissure width following oxaliplatin treatment. Consistently, a previous study did not find increases in GS in animals following nerve ligation in the hind limbs of mice (Langford et al., 2010). However, in different studies, the GS was increased in animals following infraorbital nerve ligation (Akintola et al., 2017) and in a model of cervical radiculopathy (Philips et al., 2017). It will be interesting in our future studies to examine whether the quantitative orbital tightening described in the present study can capture spontaneous pain events in these two models (Philips et al., 2017; Akintola et al., 2017) and other more prominent spontaneous pain models. Although we did not observe significant orbital tightening in the oxaliplatin-treated mice, we found that orbital tightening occurred for approximately 1 min immediately after tactile stimulation. This result indicated that our quantitative orbital tightening could be used for assessing neuropathic pain manifested as mechanical allodynia in animals with chemotherapy-induced neuropathy.

In conclusion, our quantitative orbital tightening for pain assessment with the use of machine learning with DeepLabCut provides a useful tool for investigating ongoing pain, pain induced by an optogenetic approach, and chemotherapy-induced neuropathic pain manifested by mechanical allodynia. In our future studies, it will be interesting to determine whether this new approach can allow us to assess pain in various animal pain models, including tissue and nerve injury in orofacial regions and other parts of the body. An important issue that needs to be addressed in future studies is whether we can quantify the severity of pain and the intensity of noxious stimulation, and whether the effects of well-established analgesics for pathological pain can be measured by the quantitative orbital tightening method.

Author contributions

J.G.G. conceived the research project and designed experiments. A.Y. helped set up DeepLabCut to measure orbital tightening. S.G. performed experiments. S.G. and J.L. created and maintained the transgenic mice. S.G. and J.G.G. analyzed data and participated in data interpretation. J. G.G. and SG wrote the paper.

CRediT authorship contribution statement

Saurav Gupta: Writing – original draft, Methodology, Data curation. **Akihiro Yamada:** Software, Methodology. **Jennifer Ling:** Resources, Investigation. **Jianguo G. Gu:** .

Declaration of competing interest

The authors declare that they have no known competing financial interests or personal relationships that could have appeared to influence the work reported in this paper.

Data availability

Data will be made available on request.

Acknowledgment

We thank Dr. R. Vaden for his thoughtful input on the data analysis of orbital tightening. This study was supported by NIH grants NS109059, DE018661, and DE023090 to J.G.G.

References

Abd-Elsayed, A.A., Ikeda, R., Jia, Z.F., Ling, J., Zuo, X.Z., Li, M., et al., 2015. KCNQ channels in nociceptive cold-sensing trigeminal ganglion neurons as therapeutic targets for treating orofacial cold hyperalgesia. Molecular Pain. 11 doi: ARTN 45 10.1186/s12990-015-0048-8. PubMed PMID: WOS:000358709200001.

Akintola T, Raver C, Studlack P, Uddin O, Masri R, Keller A. The grimace scale reliably assesses chronic pain in a rodent model of trigeminal neuropathic pain. Neurobiol Pain. 2017;2:13-7. Epub 20171101. doi: 10.1016/j.ynpai.2017.10.001. PubMed PMID: 29450305; PubMed Central PMCID: PMCPMC5808980.

Andresen N, Wollhaf M, Hohlbaum K, Lewejohann L, Hellwich O, Thone-Reineke C, et al. Towards a fully automated surveillance of well-being status in laboratory mice using deep learning: Starting with facial expression analysis. PLoS One. 2020;15(4): e0228059. Epub 20200415. doi: 10.1371/journal.pone.0228059. PubMed PMID: 32294094; PubMed Central PMCID: PMCPMC7159220.

Argyriou, A.A., Polychronopoulos, P., Iconomou, G., Chroni, E., Kalofonos, H.P., 2008. A review on oxaliplatin-induced peripheral nerve damage. Cancer Treat Rev. 34 (4), 368–377. https://doi.org/10.1016/j.ctrv.2008.01.003. PubMed PMID: WOS: 000256811200007.

Arnold B, Ramakrishnan R, Wright A, Wilson K, VandeVord PJ. An automated rat grimace scale for the assessment of pain. Sci Rep. 2023;13(1):18859. Epub 20231101. doi: 10.1038/s41598-023-46123-x. PubMed PMID: 37914795; PubMed Central PMCID: PMCPMC10620195.

Bidgood R, Zubelzu M, Ruiz-Ortega JA, Morera-Herreras T. Automated procedure to detect subtle motor alterations in the balance beam test in a mouse model of early Parkinson's disease. Sci Rep. 2024;14(1):862. Epub 20240109. doi: 10.1038/s41598-024-51225-1. PubMed PMID: 38195974; PubMed Central PMCID: PMCPMC10776624.

Caterina MJ, Schumacher MA, Tominaga M, Rosen TA, Levine JD, Julius D. The capsaicin receptor: a heat-activated ion channel in the pain pathway. Nature. 1997; 389(6653):816-24. Epub 1997/12/31 23:16. doi: 10.1038/39807. PubMed PMID: 9349813.

Craig KD, Prkachin, K. M., & Grunau, R. E. . The facial expression of pain. In: D. C. T, R., Melzack editor. Handbook of Pain Assessment. 2nd ed. New York: Guilford Press; 2001. pp. 153-69.

Dalla Costa E, Minero M, Lebelt D, Stucke D, Canali E, Leach MC. Development of the Horse Grimace Scale (HGS) as a pain assessment tool in horses undergoing routine castration. PLoS One. 2014;9(3):e92281. Epub 20140319. doi: 10.1371/journal.pone.0092281. PubMed PMID: 24647606; PubMed Central PMCID: PMCPMC3960217.

Deuis JR, Dvorakova LS, Vetter I. Methods Used to Evaluate Pain Behaviors in Rodents. Front Mol Neurosci. 2017;10:284. Epub 20170906. doi: 10.3389/fnmol.2017.00284. PubMed PMID: 28932184; PubMed Central PMCID: PMCPMC5592204.

Di Giminiani P, Brierley VL, Scollo A, Gottardo F, Malcolm EM, Edwards SA, et al. The Assessment of Facial Expressions in Piglets Undergoing Tail Docking and Castration: Toward the Development of the Piglet Grimace Scale. Front Vet Sci. 2016;3:100. Epub 20161114. doi: 10.3389/fvets.2016.00100. PubMed PMID: 27896270; PubMed Central PMCID: PMCPMC5107875.

Dooley JC, Glanz RM, Sokoloff G, Blumberg MS. Self-Generated Whisker Movements Drive State-Dependent Sensory Input to Developing Barrel Cortex. Curr Biol. 2020; 30(12):2404-10 e4. Epub 20200514. doi: 10.1016/j.cub.2020.04.045. PubMed PMID: 32413304; PubMed Central PMCID: PMCPMC7314650.

Gupta S, Ling J, Gu J. Assessment of orofacial nociceptive behaviors of mice with the sheltering tube method: Oxaliplatin-induced mechanical and cold allodynia in orofacial regions. Mol Pain. 2024:17448069241261687. Epub 20240531. doi: 10.1177/17448069241261687. PubMed PMID: 38818803.

Hager C, Biernot S, Buettner M, Glage S, Keubler LM, Held N, et al. The Sheep Grimace Scale as an indicator of post-operative distress and pain in laboratory sheep. PLoS One. 2017;12(4):e0175839. Epub 20170419. doi: 10.1371/journal.pone.0175839. PubMed PMID: 28422994; PubMed Central PMCID: PMCPMC5396914.

Holden E, Calvo G, Collins M, Bell A, Reid J, Scott EM, et al. Evaluation of facial expression in acute pain in cats. J Small Anim Pract. 2014;55(12):615-21. Epub 20141030. doi: 10.1111/jsap.12283. PubMed PMID: 25354833.

Kilo S, HardingRose C, Hargreaves KM, Flores CM. Peripheral CGRP release as a marker for neurogenic inflammation: a model system for the study of neuropeptide secretion in rat paw skin. Pain. 1997;73(2):201-7. Doi: 10.1016/S0304-3959(97)00108-5. PubMed PMID: WOS:A1997YK33800010.

Langford DJ, Bailey AL, Chanda ML, Clarke SE, Drummond TE, Echols S, et al. Coding of facial expressions of pain in the laboratory mouse. Nat Methods. 2010;7(6):447-9. Epub 20100509. doi: 10.1038/nmeth.1145PubMed PMID: 20453868.

Mathis A, Mamidanna P, Cury KM, Abe T, Murthy VN, Mathis MW, et al. DeepLabCut: markerless pose estimation of user-defined body parts with deep learning. Nat Neurosci. 2018;21(9):1281-9. Epub 20180820. doi: 10.1038/s41593-018-0209-y. PubMed PMID: 30127430.

McCoy ES, Park SK, Patel RP, Ryan DF, Mullen ZJ, Nesbitt JJ, et al. Development of PainFace software to simplify, standardize, and scale up mouse grimace analyses. Pain. 2024;165(8):1793-805. Epub 20240213. doi: 10.1097/j.pain.0000000000003187. PubMed PMID: 39024163.

Mykins M, Bridges B, Jo A, Krishnan K. Multidimensional Analysis of a Social Behavior Identifies Regression and Phenotypic Heterogeneity in a Female Mouse Model for Rett Syndrome. J Neurosci. 2024;44(12). Epub 20240320. doi: 10.1523/JNEUROSCI.1078-23.20PubMed PMID: 38199865; PubMed Central PMCID: PMCPMC10957218.

Nath T, Mathis A, Chen AC, Patel A, Bethge M, Mathis MW. Using DeepLabCut for 3D markerless pose estimation across species and behaviors. Nat Protoc. 2019;14(7):

2152-76. Epub 20190621. doi: 10.1038/s41596-019-0176-0. PubMed PMID: 31227823.

Oliver V, De Rantere D, Ritchie R, Chisholm J, Hecker KG, Pang DS. Psychometric assessment of the Rat Grimace Scale and development of an analgesic intervention score. PLoS One. 2014;9(5):e97882. Epub 20140516. doi: 10.1371/journal.pone.0097882. PubMed PMID: 24838111; PubMed Central PMCID: PMCPMC4024023.

Onuma K, Watanabe M, Sasaki N. The grimace scale: a useful tool for assessing pain in laboratory animals. Exp Anim. 202Epub 20240222. doi: 10.1538/expanim.24-0010. PubMed PMID: 38382945.

Philips, B.H., Weisshaar, C.L., Winkelstein, B.A., 2017. Use of the Rat Grimace Scale to Evaluate Neuropathic Pain in a Model of Cervical Radiculopathy. Comp Med. 67 (1), 34–42. PubMed PMID: 28222837; PubMed Central PMCID: PMCPMC5310623.

Piotrowski D, Clemensson EKH, Nguyen HP, Mark MD. Phenotypic analysis of ataxia in spinocerebellar ataxia type 6 mice using DeepLabCut. Sci Rep. 2024;14(1):8571. Epub 20240413. doi: 10.1038/s41598-024-59187-0. PubMed PMID: 38609436; PubMed Central PMCID: PMCPMC11014858.

Prkachin, K.M., 1992. The consistency of facial expressions of pain: a comparison across modalities. Pain. 51 (3), 297–306. https://doi.org/10.1016/0304-3959(92)90213-U. PubMed PMID: 1491857.

Reddy P, Vasudeva J, Shah D, Prajapati JN, Harikumar N, Barik A. A Deep-Learning Driven Investigation of the Circuit Basis for Reflexive Hypersensitivity to Thermal Pain. Neuroscience. 2023;530:158-72. Epub 20230826. doi: 10.1016/j.neuroscience.2023.08.023. PubMed PMID: 37640138.

Sotocinal SG, Sorge RE, Zaloum A, Tuttle AH, Martin LJ, Wieskopf JS, et al. The Rat Grimace Scale: a partially automated method for quantifying pain in the laboratory rat via facial expressions. Mol Pain. 2011;7:55. Epub 20110729. doi: 10.1186/1744-8069-7-55. PubMed PMID: 21801409; PubMed Central PMCID: PMCPMC3163602.

Tuttle AH, Molinaro MJ, Jethwa JF, Sotocinal SG, Prieto JC, Styner MA, et al. A deep neural network to assess spontaneous pain from mouse facial expressions. Mol Pain. 2018;14:1744806918763658. doi: 10.1177/1744806918763658. PubMed PMID: 29546805; PubMed Central PMCID: PMCPMC5858615.

Yamada A, Yamada AI, Ling J, Furue H, Luo W, Gu JG. Properties of Nav1.8(ChR2)-positive and Nav1.8(ChR2)-negative afferent mechanoreceptors in the hindpaw glabrous skin of mice. Mol Brain. 2023;16(1):27. Epub 20230307. doi: 10.1186/s13041-023-01015-z. PubMed PMID: 36882762; PubMed Central PMCID: PMCPMC9990257.

Yamada, A., Yamada, A., Ling, J., Furue, H., Gu, J.G., 2024. Effects of inflammation on the properties of Nav1.8-ChR2-positive and Nav1.8-ChR2-negative afferent mechanoreceptors in the hindpaw glabrous skin of mice. Mol Pain. 20 https://doi.org/10.1177/17448069241240452. PubMed PMID: 38438192; PubMed Central PMCID: PMCPMC10960352.

Zhang EQ, Leung VS, Pang DS. Influence of Rater Training on Inter- and Intrarater Reliability When Using the Rat Grimace Scale. J Am Assoc Lab Anim Sci. 2019;58(2):178-83. Epub 201902doi: 10.30802/AALAS-JAALAS-18-000044. PubMed PMID: 30755291; PubMed Central PMCID: PMCPMC6433356.